

Evidence of Ferrimagnetism in Ferromagnetic $\text{La}_{0.67}\text{Ca}_{0.33}\text{MnO}_3$ nanoparticle

R.N. Bhowmik*

Department of Physics, Pondicherry University,

R.V. Nagar, Kalapet, Pondicherry-605014, India

The present report is dedicated to show that ferromagnetic $\text{La}_{0.67}\text{Ca}_{0.33}\text{MnO}_3$ (LCMN) particles can be better described in the framework of ferrimagnetic model. To confirm the ferrimagnetic signature in ferromagnetic LCMN particles, the temperature dependence of the inverse of magnetic susceptibility in the paramagnetic state of the samples was taken as a tool of data analysis. The observed ferrimagnetism is understood as an effect of the core-shell spin structure in LCMN particles.

Key Words: A. Ferromagnetic nanoparticle; B. Mechanical Milling; C. Ferrimagnetism; D. Core-shell spin structure

PACS:75.47.Lx,75.30.Cr,75.50.-y,75.50.Gg,75.50.Tt

I. INTRODUCTION

Magnetic nanomaterials are continued to be at the center of current research interests due to their huge technological applications and incomplete understanding of many discovered phenomena. For example, superparamagnetic blocking of magnetic moments below the conventional paramagnetic to ferromagnetic transition temperature (T_C), appearance of unconventional spin glass behaviour at lower temperatures, decrease of effective magnetic moment of the material, exchange bias effect, quantum tunnelling of magnetization, and low field magnetoresistance have been observed when the particle size of ferromagnetic materials decreases into nanosize dimension (below 100 nm)[1, 2]. Various mechanisms have been introduced in literature to describe the magnetic features of nanoparticles, e.g., core-shell

* E-mail address for correspondence:
rnbhowmik.phy@pondiuni.edu.in

structure, dipole interactions, inter-particle interactions, exchange anisotropy [3]. Among the proposed mechanisms, the core-shell concept is world wide accepted to explain the features of nanoparticle magnetism. In a magnetic nanoparticle the central part, known as core, is assumed to be identical to the structure and property of bulk material with micron sized particles. The structure and property of the outer part of the particle, known as shell, are drastically different in comparison with core [3, 4]. If the bulk material is a typical long ranged ferromagnet (antiferromagnet), then core is assumed to be long ranged ferromagnet(antiferromagnet) and disorder is introduced in the shell part of the particle. This means the property of a magnetic nanoparticle is basically heterogeneous in character (i.e., consisting of two different magnetic components or equivalent to two magnetic sublattices) over a length of particle dimension and also in the whole dimension of the material when the particles are in contact. The common phenomena due to the heterogeneous magnetic structure in ferromagnetic nanoparticles are the reduction of particle moment and magnetic blocking/freezing at lower temperatures. On the other hand, antiferromagnetic nanoparticles have shown many enhanced properties mainly due to different magnetic structure of shell part in comparison with bulk counter material [4]. This shows that core-shell structure plays an important role in the properties of magnetic materials, immaterial of ferromagnetic or antiferromagnetic particles. Hence, proper understanding of the effects of core-shell structure is not only the long standing problem, but also useful in designing the application oriented materials. To understand the effects of core-shell structure in different types heterogeneous magnetic structures, e.g., ferromagnetic core is surrounded by antiferromagnetic/paramagnetic/ferrimagnetic shell or antiferromagnetic core is surrounded by ferromagnetic/ferrimagnetic shell have been synthesized and reported in literature [5–8]. The effect of shell disorder and spin frustration has also been discussed in many spin-bilayer magnetic systems [3]. G. Bouzear et al. [9] discussed the effect of competition between introduced superexchange (antiferromagnetic) interactions in long ranged double exchange ferromagnetic matrix. They argued that in the lower limit of antiferromagnetic superexchange interactions the long ranged ferromagnetic state is not altered significantly; rather a canted ferromagnetic phase or induced new magnetic phase is appeared in the spin system. The induced magnetic phases may be either stable or unstable depending on the quantum of magnetic disorder and frustration. Some report also studied core-shell structure in a composite material consisting of ferrimagnetic core and ferroelectric shell [10].

Recently, $\text{La}_{0.67}\text{Ca}_{0.33}\text{MnO}_3$ nanoparticles in crystalline and amorphous structural phases have shown many interesting magnetic properties, related to magnetic disorder at core-shell structure of the particles [11]. A proper knowledge of magnetic interactions between core-shell spins would be useful not only to realize the colossal magnetoresistance and inter-grain tunneling of polarized spins, but also relevant to realize the effect of disorder on double exchange ferromagnetism in manganites. In the present work, we demonstrate that the modified magnetism in ferromagnetic $\text{La}_{0.67}\text{Ca}_{0.33}\text{MnO}_3$ nanoparticles is identical to the typical features of ferrimagnetic materials. The evidence of ferrimagnetic signature in $\text{La}_{0.67}\text{Ca}_{0.33}\text{MnO}_3$ nanoparticles is also discussed by comparing the features already observed in ferrimagnetic ($\text{Mn}_{0.5}\text{Ru}_{0.5}\text{Co}_2\text{O}_4$ and MnCr_2O_4) particles.

II. EXPERIMENTAL

Details of the sample preparation of $\text{La}_{0.67}\text{Ca}_{0.33}\text{MnO}_3$ (perovskite) particles and their characterization have been reported elsewhere [11]. In brief, the polycrystalline bulk $\text{La}_{0.67}\text{Ca}_{0.33}\text{MnO}_3$ sample was prepared by solid state sintering (maximum temperature 1380°C) method. The bulk sample was subjected to mechanical milling in Argon atmosphere upto 200 hours using Fritsch Planetary Mono Mill "Pulverisette 6" to synthesize the material in nanocrystalline and amorphous phase. The structural phase of the samples was confirmed from room temperature XRD spectrum. The XRD spectrum indicated that crystalline nature of the material decreases significantly for the milling time more than 61 hours and amorphous phase dominates in the spectrum for milling time more than 98 hours. Both bulk and milled samples (upto mh98) are in similar crystallographic phase and found to be matching with orthorhombic structure with Pnma space group. The temperature dependence of magnetization under zero field cooled condition was measured using SQUID magnetometer (MPMS-Quantum Design, USA). The temperature dependence of dc magnetization at 100 Oe in the temperature range 100 K to 400 K was also reproduced using vibrating sample magnetometer (Lakeshore 7404 model).

III. EXPERIMENTAL RESULTS

Details of the temperature and field dependence of dc magnetization have been reported elsewhere [11]. In summary, the paramagnetic to ferromagnetic Curie temperature (T_C) for bulk (LCMN) sample is nearly 281 K and T_C decreases to 262 K, 250 K, 238 K, 225 K and 212 K for mechanical milled mh25(nanocrystalline, particle size ~ 65 nm), mh61 (nanocrystalline, particle size ~ 12 nm), mh98 (nanocrystalline+amorphous, particle size ~ 16 nm), mh146 (amorphous, particle size ~ 60 nm) and mh200 (amorphous, particle size ~ 90 nm) samples. At the same time, the long ranged ferromagnetic order (spontaneous magnetization $\sim 3.6 \mu_B$) of bulk LCMN sample decreases to 2.17, 0.87, 0.35, 0.17, 0.10 (in μ_B) unit) for mh25, mh61, mh98, mh146 and mh200 samples, respectively. These are some typical features of the magnetic disorder effect in ferromagnetic materials. In the present paper, we would like to show some specific magnetic features of the samples based on magnetization data at (higher temperature) paramagnetic regime. In Fig. 1, the dc magnetic susceptibility ($\chi_{dc} = M/H$) of bulk LCMN sample sharply increases above the magnetization peak temperature $T_p \sim 260$ K. On the other hand, magnitude of susceptibility, as well as sharp increase of magnetization below the respective T_C systematically decreases for mh25, mh98 and mh200 samples. The decrease of the χ (T) variation in milled samples reflects the increasing magnetic disorder in the ferromagnetic material and realized in the previous work [11]. Interestingly, a typical ferrimagnetic sample, e.g., $Mn_{0.5}Ru_{0.5}Co_2O_4$ (RuMn) spinel oxide in the inset of Fig. 1, also exhibits the similar χ_{dc} (T) behaviour above its magnetization peak temperature $T_p \sim 100$ K. This means only the shape of χ_{dc} (T) curve in the paramagnetic state can not determine the nature of magnetic order in the samples, whether ferromagnet or ferrimagnet. The nature of magnetic order can be confirmed in convincing manner from the temperature dependence of the inverse of magnetic susceptibility in the paramagnetic state. For this purpose, we extended the dc magnetization measurement up to 400 K. First, we confirm the difference of the temperature dependence of the inverse of susceptibility curve in paramagnetic regime between bulk LCMN (ferromagnetic) and RuMn (ferrimagnetic) samples. Fig. 2 shows that the inverse of dc susceptibility ($\chi_{dc}^{-1} = H/M$) data for bulk LCMN sample at high temperatures ($T \geq 300$ K) are fitted with a simple Curie-Weiss law:

$$\chi = C/(T - \theta_w) \quad (1)$$

Application of this equation confirms the ferromagnetic order in bulk LCMN sample. The obtained parameters are Curie constant ($C \sim 0.0196$) and paramagnetic Curie temperature ($\theta_w \sim + 270$ K). In contrast, the inverse of dc susceptibility (χ^{-1}) for $\text{Mn}_{0.5}\text{Ru}_{0.5}\text{Co}_2\text{O}_4$ spinel oxide at high temperatures is fitted with a typical equation:

$$1/\chi = (T - \theta_1)/C_{eff} - \xi/(T - \theta_2) \quad (2)$$

In general, this equation is applicable for ferrimagnet [12]. The obtained parameters ($\theta_1 \sim -1320$ K, $C_{eff} \sim 0.076$, $\xi \sim 200850$, $\theta_2 \sim + 112$ K), in particular the positive value of θ_2 (slightly larger than $T_C \sim 100$ K) and a high negative value of θ_1 , clearly indicate the ferrimagnetic order in $\text{Mn}_{0.5}\text{Ru}_{0.5}\text{Co}_2\text{O}_4$ spinel oxide. Similar (χ_{dc}^{-1} (T)) character was also noted in many other ferrimagnetic materials [12, 13].

Now, we analyze the temperature dependence of the inverse of dc susceptibility data for mechanical milled nanoparticle samples. As shown in Fig. 3, the data are well fitted with a simple Curie-Weiss law (equation (1)) above 330 K. The fit parameters of Curie-Weiss law (C and θ_w) are shown in Table I. On the other hand, the hyperbolic shape of χ^{-1} (T) curves (with down curvature) above the Curie temperature of the samples suggests that milled samples belong to the class of either ferrimagnet or double exchange ferromagnet [14]. We noted that the χ^{-1} (T) curves of the present nanoparticle samples are identical to the ferromagnetic MnCr_2O_4 nanoparticle samples [13]. To clarify the ferrimagnetic nature of the nanoparticle (NP) samples, we have fitted the χ^{-1} (T) data in the temperature range 330 K-400 K using equation (2). We followed a non-linear curve fitting method. Initially, the parameters (θ_1 , C_{eff} , ξ and θ_2) were allowed to take initial values and iterated 10 times. As soon as the fitted curve comes close to the experimental curve, we start to restrict the parameters one by one. Finally, best fit curve was obtained by allowing all parameters to vary, except θ_2 keeping constant. The experimental data in the paramagnetic state of the samples fitted with equation (2) are shown in Fig. 3. The fit on susceptibility data in the paramagnetic regime according to equation (2) is excellent. The fit parameters are shown in Table I. A comparative fits applying equation (1) and (2) for mh98 and mh200 samples suggests that equation (1) may be well valid at higher temperature, but equation (2) is more appropriate to describe the magnetic behaviour over a wide temperature range above T_C . We noted using equation (1) that the paramagnetic Curie temperature (θ_w) systematically decreases as the material transforms from bulk polycrystalline phase to nanocrystalline (NC)

phase and then, to amorphous (AMP) phase. The θ_w values remained positive for bulk as well as mh25, mh61 and mh98 samples, where as θ_w becomes negative for mh146 and mh200 samples. The negative value of θ_w indicates the introduction of antiferromagnetic exchange interactions in the material as the particle size and crystalline phase changed. As discussed in earlier report [11], the magnetic dynamics of the present material strongly depends on the structural phase transformation, rather than the particle size effects. The θ_1 (obtained using equation (2)) also follows the pattern of θ_w , showing positive values only for mh25 and mh61 samples. The spin glass like feature in amorphous (mh146) sample clearly proves the the reduction of ferromagnetic (FM) exchange interactions or development of antiferromagnetic (AFM) exchange interactions in nanocrystalline and amorphous samples, because spin glass like feature needs sufficient amount of both magnetic disorder and competition between FM/AFM interactions. On the other hand, θ_2 is always positive and change is not drastic (within 9 K considering all milled samples). The positive value of θ_2 suggested the retaining of a strong double exchange ferromagnetic interactions [14] both in nanocrystalline and amorphous phase of $\text{La}_{0.67}\text{Ca}_{0.33}\text{MnO}_3$ nanoparticles [11]. At the same time, application of equation (2) suggests the ferrimagnetic character of mechanical milled nanoparticle LCMN samples. Similar magnetic behaviour was also observed in ferrimagnetic MnCr_2O_4 nanoparticles [13]. Some reports [15, 16] also attempted to explain the magnetization data in the paramagnetic regime of ferromagnetic nanomaterials by following a simple Curie-Weiss law (equation (1)), but those data seem to be more appropriate to the ferrimagnetic description (equation (2)).

The validity of ferrimagnetic equation (2) in our milled samples can be examined by considering the core-shell spin structure of nanoparticles, already proposed in earlier work [11]. The existence of strong ferromagnetic order, even in the nanocrystalline and amorphous phase, is essentially due to ferromagnetic ordered core spins. On the other hand, magnetic disorder is confined mainly in the shell part for nanocrystalline particles (NCR NP) and also introduces in the core part for amorphous nanoparticles (AMP NP). The shell spins may not be typical antiparallel with respect to core, but effective spin moment of shell is obviously low in comparison with ferromagnetic core and schematically shown in Fig.4. Similar magnetic modulation was previously proposed for antiferromagnetic nanoparticle [4] and later applied for ferromagnetic manganite nanoparticles [17]. This allows us to consider the magnetic contributions form shell and core of a nanoparticle equivalent to two unequal

magnetic sublattices (shown in lower diagram of Fig. 4), as usually seen in a typical long ranged ferrimagnet. It must be differentiated that two different magnetic sublattices as we suggest here for the ferromagnetic particles is not due to different crystal environments, i.e., tetrahedral and octahedral lattice sites of a typical ferrite consisting of two magnetic sublattices of antiparallel directions [12, 13]. Based on the experimental observations, the concept of two different magnetic structure could be a realistic approach for describing the magnetic properties of ferromagnetic nanomaterials. Recently, similar concept was modelled by C.R.H. Bahl et al. [5] and M. Vasilakaki et al. [6].

IV. CONCLUSIONS

$\text{La}_{0.67}\text{Ca}_{0.33}\text{MnO}_3$ ferromagnet exhibited many interesting features in the nanocrystalline and amorphous phase, as an effect of increasing disorder in core-shell spin morphology and lattice structure. The present work clearly provides the evidence of ferrimagnetic character in ferromagnetic $\text{La}_{0.67}\text{Ca}_{0.33}\text{MnO}_3$ (LCMN) nanoparticles. The ferrimagnetic concept, as proposed in this work, is interesting and could be applied for the understanding of basic mechanism in many ferromagnetic nanoparticles. Especially, this approach could be more effective for the proper demonstration of the effect of core-shell spin structure in ferromagnetic nanoparticles.

Acknowledgement: We thank A. Poddar of Saha Institute of Nuclear Physics and CIF, Pondicherry University for magnetic measurements.

-
- [1] A.P. Ramirez, S. W. Cheong, and P. Schiffer, *J. Appl. Phys.* **81**, 5337 (1997).
 - [2] S.P. Gubin, Y.A. Koksharov, G.B. Khomutov and G. Y. Yurkov, *Russ. Chem. Rev.* **74**, 489 (2005).
 - [3] O. Iglesias, A.Labarta, and X. Batlle, *J. Nanoscience and Nanotech.* **8**, 2761 (2008).
 - [4] R.N. Bhowmik, R. Nagarajan, and R. Ranganathan, *Phys. Rev. B* **69**, 054430 (2004).
 - [5] C.R.H. Bahl, J. Garde1., K. Lefmann, T.B.S. Jensen, P.-A. Lindg, D.E. Madsen, and S. Mrup, *Eur. Phys. J. B* **62**, 53 (2008).
 - [6] M. Vasilakaki and K. N. Trohidou, *Phys. Rev. B* **79**, 144402 (2009).

- [7] M. Muroi, P.G. McCormick and R. Street, *Rev. Adv. Matter. Sci.* **5**, 76 (2003).
- [8] O. Masala and R. Seshadri, *J. Am. Chem. Soc.* **127**, 9354 (2005).
- [9] G. Bouzerar, R. Bouzerar, and O. Cpas, *Phys. Rev. B* **76**,144419 (2007).
- [10] V. Corral-Flores, D. Bueno-Baques, D. Carrillo-Flores, and J.A. Matutes-Aquino, *J. Appl. Phys.* **99**, 08J503 (2006).
- [11] R. N. Bhowmik, A.Poddar, R. Ranganathan, and Chandan Mazumdar, *J. Appl. Phys.* **105**, 113909 (2009).
- [12] J. S. Smart, *Am. J. Phys.* **23**, 356 (1955).
- [13] R.N. Bhowmik, R. Ranganathan, and R. Nagarajan, *Phys. Rev. B* **73**, 144413(2006).
- [14] P.W. Anderson and H. Hasegawa *Phys. Rev.* **100**, 675 (1955).
- [15] Y. H. Huang, J. Linden, H. Yamauchi, and M.Karppinen,*Chem. Mater.* **16**, 4337 (2004).
- [16] X.H. Li, Y.P. Sun, W.J. Lu, R. Ang, S.B. Zhang, X.B. Zhu, W.H. Song, and J.M. Dai *Solid State Comm.* **145**, 98 (2008).
- [17] T. Zhang, T.F. Zhou, T. Quian, and X.G. Li, *Phys. Rev. B* **76**, 174415 (2007).

TABLE I: The particle size (d) of the milled samples are determined from the TEM data. The fit parameters (C and θ_w) were obtained using simple Curie-Weiss law (equation 1). The parameters (C_{eff} , θ_1 , θ_2 and ξ) were obtained using equation (2) for different milled samples. It may be mentioned that the present values of C and θ_w (K) using temperature range 330 K to 400 K are slightly different from the values $C \sim 0.0176$ and $\theta_w \sim 275$ K using temperature range 300 K to 340 K and previously reported [11].

Sample	d	C (K g Oe/emu)	θ_w (K)	C_{eff} (K g Oe/emu)	θ_1 (K)	θ_2 (K)	ξ (arb. unit)
Bulk	few μm	0.196	270	–	–	–	–
mh25	65 nm	0.0275	200	0.035(3)	120 \pm 4	251	106450 \pm 2200
mh61	12 nm	0.0365	100	0.043(2)	33 \pm 3	250	53400 \pm 520
mh98	16 nm	0.0244	20	0.043(2)	-46 \pm 4	247	91800 \pm 1000
mh146	60 nm	0.0251	-80	0.024(6)	-87 \pm 2	243	80000 \pm 1200
mh200	90 nm	0.0245	-97	0.024(3)	-106 \pm 3	242	62000 \pm 800

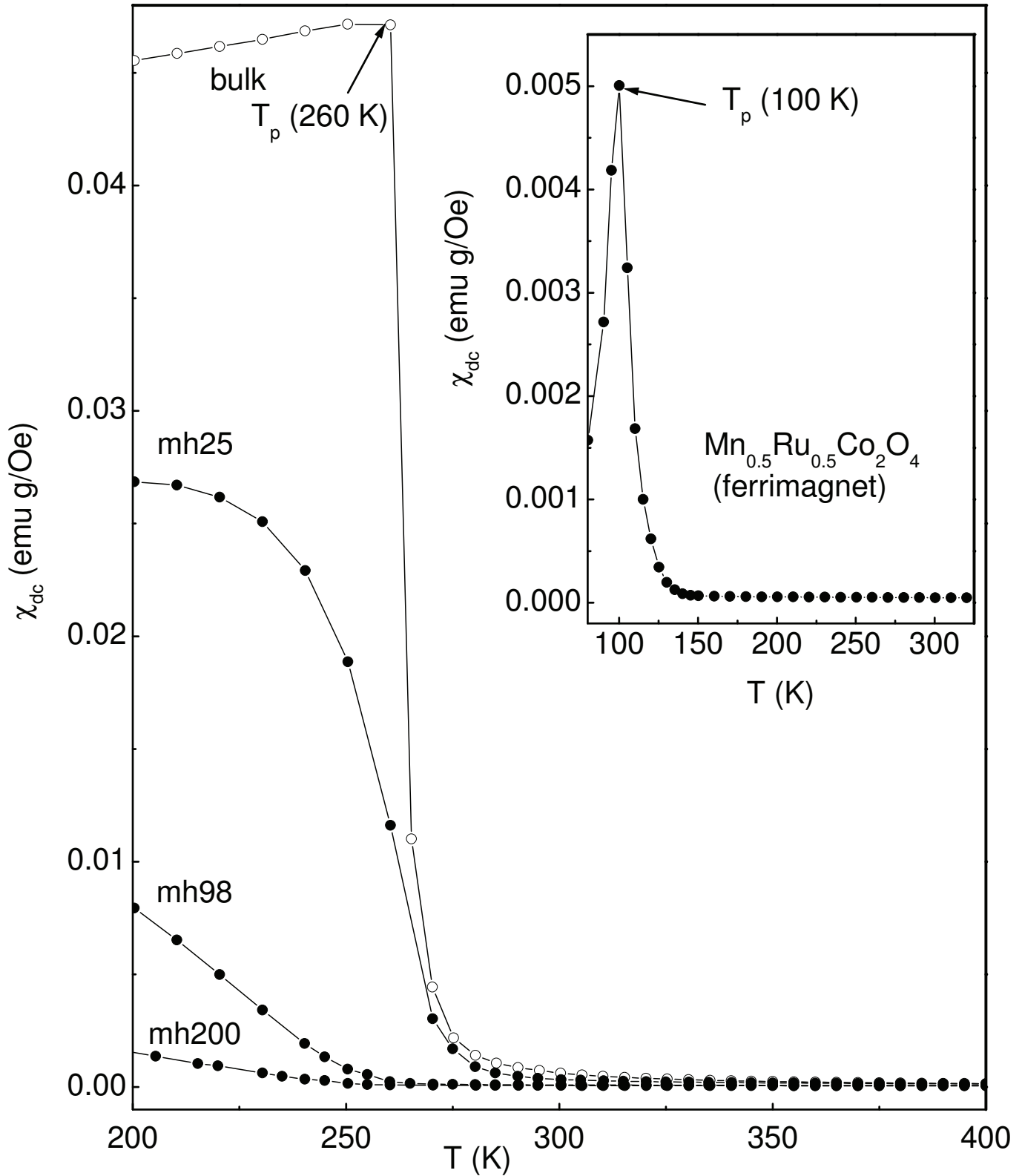


Fig.1 Temperature dependence of dc susceptibility ($\chi_{dc}(T)$) at 100 Oe for ferromagnetic (bulk) LCMN sample and selected milled samples. Inset shows the ($\chi_{dc}(T)$) data at 10 oe for ferrimagnetic $\text{Mn}_{0.5}\text{Ru}_{0.5}\text{Co}_2\text{O}_4$.

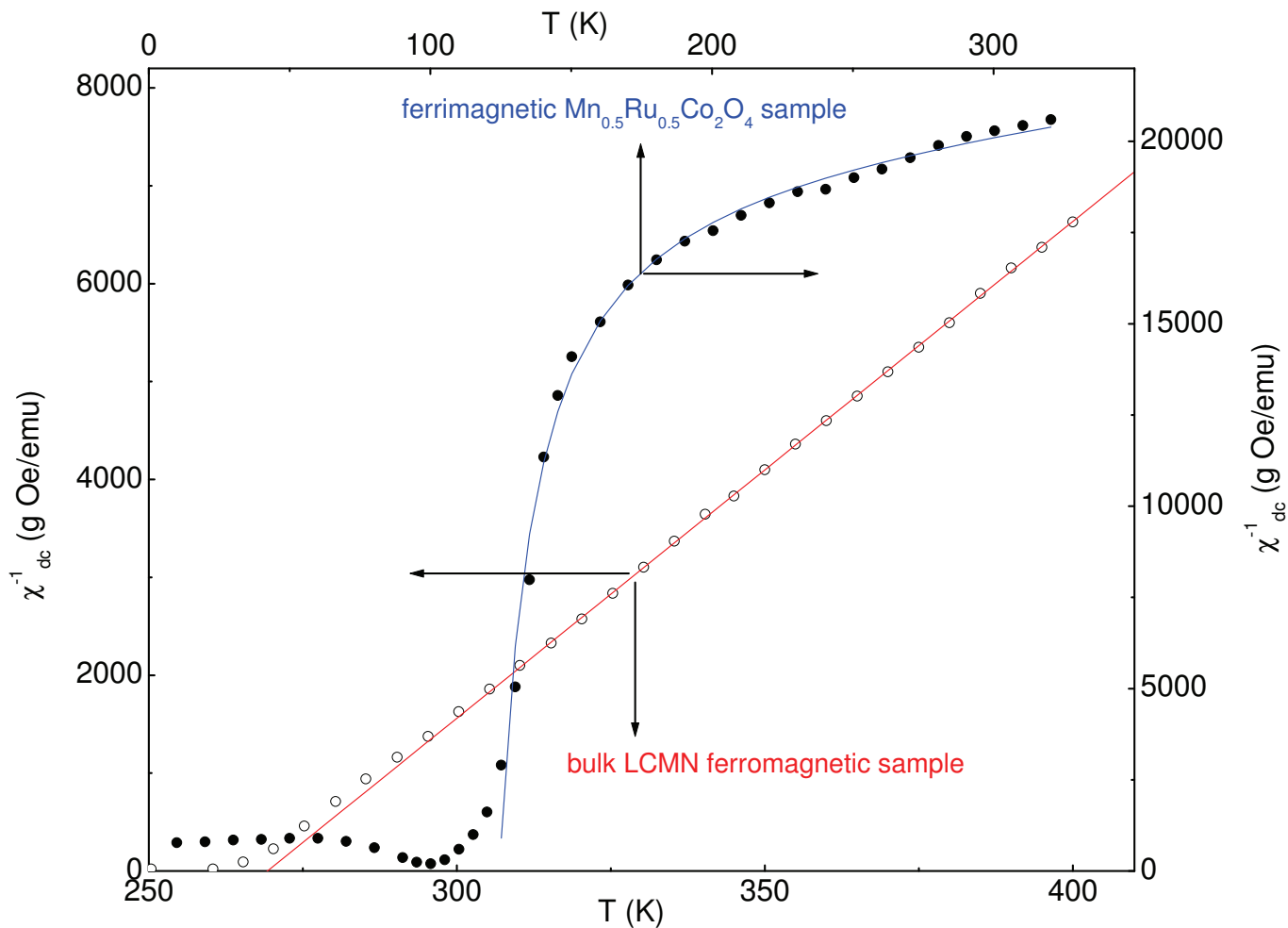


Fig. 2 (Colour online) Inverse of dc susceptibility vs. temperature data of bulk LCMN sample (left-bottom axis) and RuMn sample (right-top axis) are fitted with equation 1 (red line) and equation 2 (blue line), respectively.

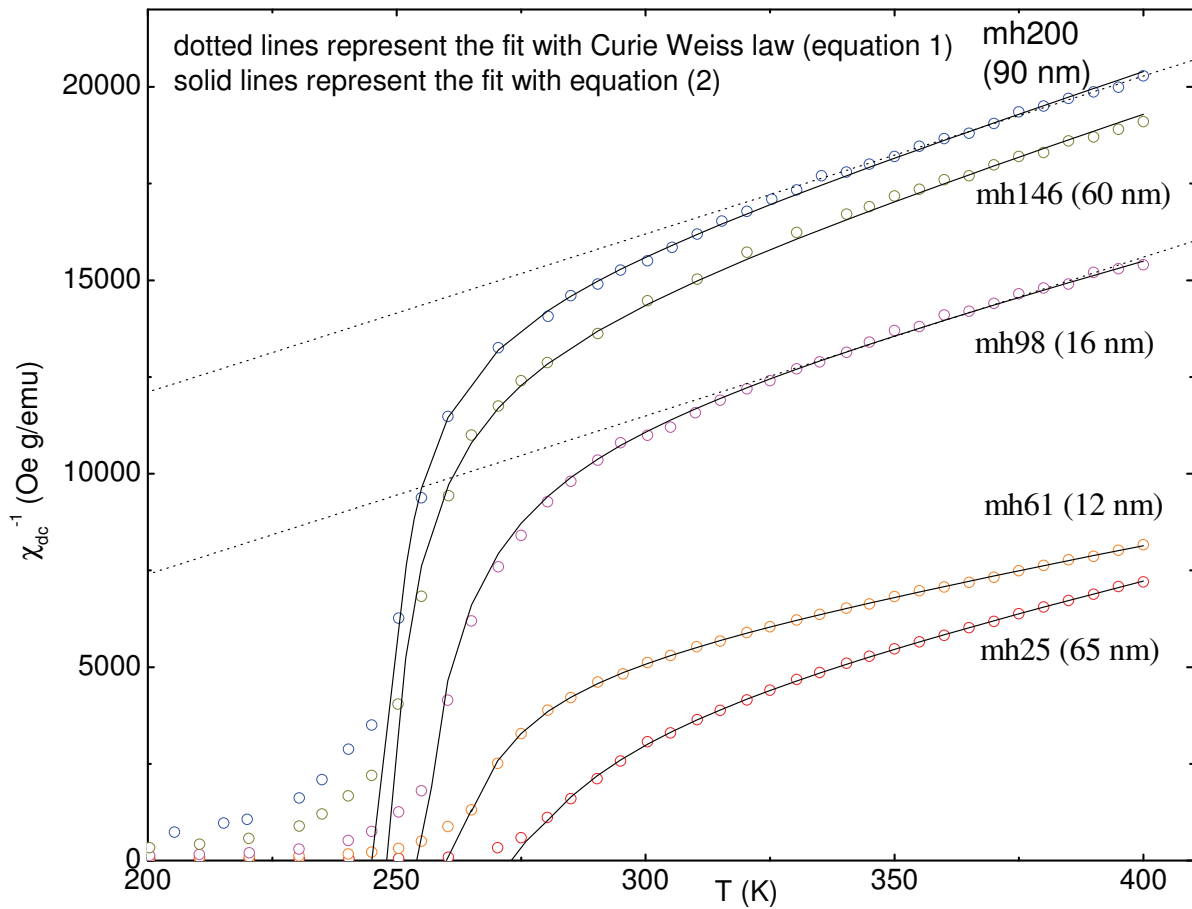


Fig. 3 (Colour online) inverse of dc susceptibility at high temperature regime for nanoparticle samples. The fit data show that Curie-Weiss law is applicable only at higher temperature, whereas equation (2) is applicable over a wide temperature range above T_c of the samples.

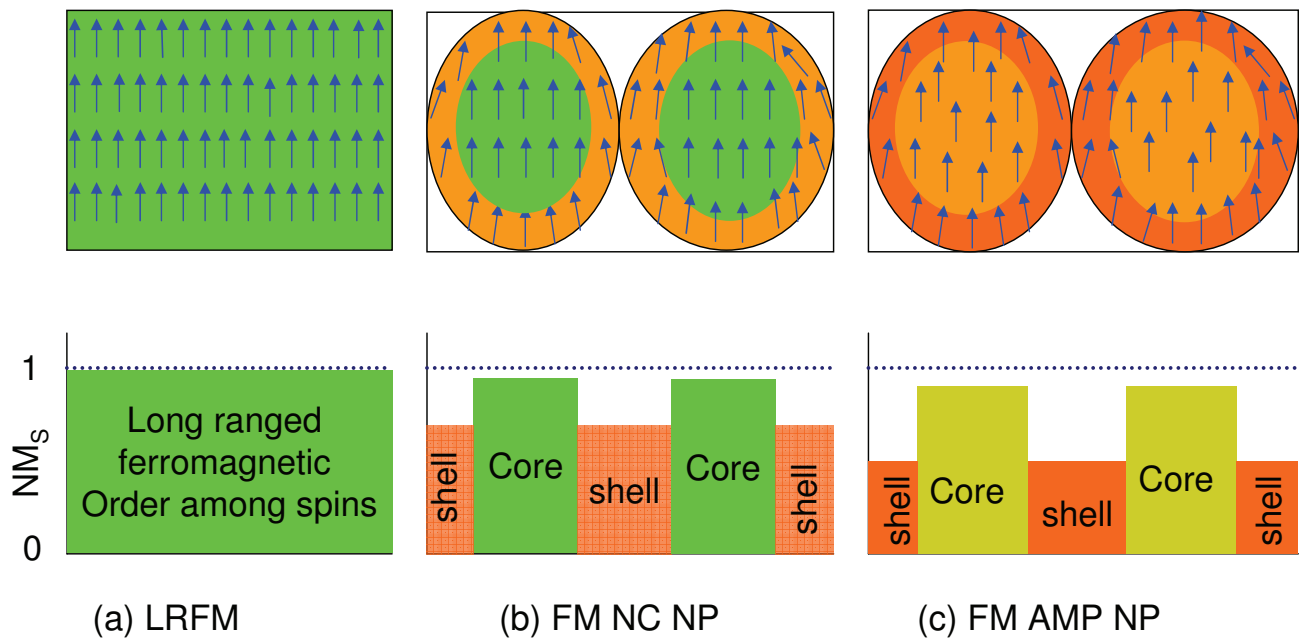


Fig. 4 (Colour online) shows a schematic diagram for long ranged ferromagnetic (LRFM) ordered spins (a), core-shell magnetic ordered spins (b), and core-shell Magnetic ordered Spins (c) in the top diagram and corresponding normalized saturation magnetization (NM_s) of different FM samples (nanocrystalline nanoparticle –NCNP, amorphous nanoparticle-AMPNP) compared to the bulk LRFM sample.